Epilepsia, 53(7):1233–1244, 2012
doi: 10.1111/j.1528-1167.2012.03525.x

FULL-LENGTH ORIGINAL RESEARCH

Hypometabolism precedes limbic atrophy and spontaneous recurrent seizures in a rat model of TLE

*Bianca Jupp, †John Williams, ‡David Binns, ‡Rodney J. Hicks, *Lisa Cardamone, *Nigel Jones, §[1]Sandra Rees, and *[1]Terence J. O'Brien

*Department of Medicine, Royal Melbourne Hospital, The University of Melbourne, Parkville, Victoria, Australia; †Florey Neuroscience Institutes, Parkville, Victoria, Australia; ‡The Centre for Molecular Imaging, Peter MacCallum Cancer Institute, East Melbourne, Victoria, Australia; and §Department of Anatomy and Cell Biology, The University of Melbourne, Parkville, Victoria, Australia

Summary

Purpose: Temporal hypometabolism on fluorodeoxyglucose positron emission tomography (FDG-PET) is a common finding in patients with drug-resistant temporal lobe epilepsy (TLE). The pathophysiology underlying the hypometabolism, including whether it reflects a primary epileptogenic process, or whether it occurs later as result of limbic atrophy or as a result of chronic seizures, remains unknown. This study aimed to investigate the ontologic relationship among limbic atrophy, histological changes, and hypometabolism in rats.

Methods: Serial in vivo imaging with FDG-PET and volumetric magnetic resonance imaging (MRI) was acquired before and during the process of limbic epileptogenesis resulting from kainic acid–induced status epilepticus in the rat. The imaging data were correlated with histologic measures of cell loss, and markers of astrogliosis (glial fibrillary acid protein [GFAP]), synaptogenesis (synaptophysin), glucose transporter 1 (Glut1) and energy metabolism (cytochrome oxidase C), on brains of the animals following the final imaging point.

Key Findings: Hippocampal hypometabolism on FDG-PET was found to be present 24 h following status epilepticus, tending to lessen by 1 week and then become more marked again following the onset of spontaneous seizures. Atrophy of limbic structures was evident from 7 days post-SE, becoming progressively more marked on serial MRI over subsequent weeks. No relationship was observed between the severity of MRI-detected atrophy or CA1 pyramidal cell loss and the degree of the hypometabolism on FDG-PET. However, an inverse relationship was observed between hypometabolism and increased expression of the Glut1 and synaptophysin in the hippocampus.

Significance: These findings demonstrate that hypometabolism occurs early in the processes of limbic epileptogenesis and is not merely a consequence of pyramidal cell loss or the progressive atrophy of limbic brain structures that follow. The hypometabolism may reflect cellular mechanisms occurring early during epileptogenesis in addition to any effects of the subsequent recurrent spontaneous seizures.

KEY WORDS: Temporal lobe epilepsy, Fluorodeoxyglucose positron emission tomography, MRI, Post–kainic acid status epilepticus, Epileptogenesis.

The majority of patients with medically refractory temporal lobe epilepsy (TLE) show prominent mesial hypometabolism in the epileptogenic temporal lobe on [^{18}F] fluorodeoxyglucose positron emission tomography (FDG-PET) (Henry et al., 1990; Theodore et al., 2001; O'Brien et al., 2008). It is notable that FDG-PET can reliably lateralize the epileptogenic hippocampus in patients who lack the typical changes of mesial temporal sclerosis on magnetic resonance imaging (MRI) (Carne et al., 2004). However the underlying pathophysiology of this hypometabolism and its relationship to epileptogenesis and the severity of TLE are largely unknown. In studies of patients with established, medically refractory TLE little relationship has been found between the severity of the hypometabolism observed on FDG-PET and other recognized pathophysiologic changes associated with TLE (O'Brien et al., 1997; Foldvary et al., 1999). However, this is still controversial. Studies of blood flow (Fink et al., 1996) and cell loss (Foldvary et al., 1999) have demonstrated a limited correlation with the degree and extent of PET-detected hypometabolism, whereas some correlation has been demonstrated between the degree of hypometabolism and epilepsy duration and number of seizures experienced (Jokeit et al., 1999; Matheja et al., 2001). Given this, it is uncertain whether the hypometabolism is a marker of the primary epileptogenic process or alternatively a secondary consequence of the chronic epilepsy. Such

Accepted March 31, 2012; Early View publication June 12, 2012.
Address correspondence to Professor Terence J. O'Brien, MB, BS, MD, FRACP, Department of Medicine, Royal Melbourne Hospital, The University of Melbourne, Parkville, 3050 Vic, Australia. E-mail: obrientj@unimelb.edu.au
[1]Both authors contributed equally to this work.

temporal and pathophysiologic relationships are difficult to study in humans because of the long duration of the disease course and the rare opportunities to image premorbid epileptic states. Traditional histologic and autoradiographic techniques in animal models are also unable to readily investigate these ontologic issues, as only one time point can be assessed in each animal.

In vivo FDG-PET imaging in animal models of epilepsy provides an opportunity to investigate the ontologic relationship among limbic hypometabolism, epileptogenesis, the effects of seizures and disease progression, and its underlying pathophysiologic basis (Dedeurwaerdere et al., 2007). To date a small number of studies have used PET to examine the acute effect of induced convulsive seizures (Kornblum et al., 2000; Mirrione et al., 2006) and limbic epileptogenesis (Goffin et al., 2009; Guo et al., 2009) in rodents. These studies have found during both kainic acid (KA) and lithium pilocarpine-induced status epilepticus that FDG uptake in the brain is increased, whereas FDG uptake is decreased during epileptogenesis following status epilepticus. Furthermore, Guo et al. (2009) found a significant relationship between the degree of hypometabolism in the entorhinal cortex early following status epilepticus and the development of later spontaneous recurrent seizures. These studies, however, failed to account for the effect of the significant limbic atrophy that occurs following status epilepticus in these models, potentially confounding measures of hypometabolism. Furthermore, no studies have investigated the relationship between imaging outcomes and postmortem histology in order to better understand the underlying cellular correlates of the hypometabolism on FDG-PET and its potential pathologic role in limbic epileptogenesis. The purpose of the current study was to use serial in vivo FDG-PET and MRI to characterize the spatiotemporal development of FDG hypometabolism during epileptogenesis in the KA-induced status epilepticus model of TLE and to correlate this with the development of the volumetric MRI and histologic changes.

Methods

Animals

The study and all procedures were approved by the animal ethics committees of The Ludwig Cancer Institute/Department of Surgery, Royal Melbourne Hospital, and the Florey Neuroscience Institutes. All procedures were performed according to the guidelines set by the Australian Code of Practice for the Prevention of Cruelty to Animals.

Twenty-three, 14- to 16-week-old male Wistar rats (breeding colony at Department of Medicine, the Royal Melbourne Hospital, The University of Melbourne, Parkville, Victoria, Australia) were implanted with custom-made gold bipolar electrodes as described previously (Jupp et al., 2006a,b) for confirmation of status epilepticus and later spontaneous recurrent seizures by EEG. Two weeks following surgery, 16 animals underwent KA administration to induce status epilepticus. Briefly, animals received repeated low-dose KA administration (Hellier et al., 1998; Hellier & Dudek, 2005) (5 mg/kg, i.p., followed by 2.5 mg/kg, i.p., injections once per hour; Ocean Produce Industries, Diggs, VA, U.S.A.) until continual epileptiform activity was observed on EEG. After 4 h, status epilepticus was terminated by injection of diazepam (2 mg/kg, i.p., every 15 min until seizure activity ceased on electroencephalography (EEG); Roche, Dee Why, NSW, Australia). Five animals died during status epilepticus and were therefore not included in the analysis. Seven control animals underwent identical surgeries, handling, and imaging but received saline in place of KA. All animals were periodically monitored post–status epilepticus via video-EEG (approximately 24 h every week for the duration of the experiment) to confirm the development of spontaneous recurrent seizures. Ongoing seizures were recorded in all animals that underwent KA-induced status epilepticus, commencing as early as 1 week after status epilepticus.

Image acquisition

Five serial FDG-PET and MRI acquisitions were acquired for each of the 18 animals (KA, n = 11; control, n = 7), over a period of 6 weeks: (1) One week after electrode implantation before status epilepticus, (2) one day following status epilepticus (24 h), (3) one week following status epilepticus (7 days), (4) three weeks following status epilepticus (21 days), and (5) five weeks following status epilepticus (35 days; 6 weeks following surgery).

Animals were fasted for 4 h before PET acquisitions to maximize glucose uptake in the brain. One hour before scanning animals were injected with between 1 and 1.5 mCi (37 and 55 MBq) of [^{18}F] FDG, i.p., to extend the time taken for the FDG to reach the brain, thereby minimizing the acute affects of handling and injection on the scan (Gonzalez-Lima, 1992), and were placed in a quiet location during the uptake period of 1 h, corresponding to the preparation of human subjects undergoing interictal FDG PET studies (O'Brien et al., 2001). Following this uptake period, animals were anesthetized using a ketamine (75 mg/kg)/xylazine (10 mg/kg) cocktail injected intraperitoneally and once immobile animals were placed within the field of view of the PET camera (Mosaic; Philips, Milpitas, CA, U.S.A.) and a half hour emission scan in frame mode was acquired. The resulting sinogram was reconstructed using an iterative, ordered-subset estimate maximization (OSEM) algorithm provided by the manufacturer to give a voxel size of $1 \times 1 \times 1$ mm. PET images were normalized to FDG uptake in the cerebellum to account for differences in activity of administered PET radioligand and normal variation in intraperitoneal tracer uptake. This region was chosen according to previous studies demonstrating that FDG uptake in this region was unaffected by status epilepticus (Goffin et al., 2009; Guo et al., 2009) or by KA administration and provided consistent uptake values on

repeated scans (Jupp B, Hicks R, Binns D, O'Brien TJ, unpublished observations). No attenuation or partial volume corrections were applied.

Within 24 h of each PET scan a volumetric T_2-weighted MRI was acquired on a 4.7 T Bruker Biospec 47/30 Avance small animal spectrometer (Ettlingen, Germany) using a shielded gradient set (Bruker Biospec) appropriate for rats as described previously (Jupp et al., 2006a). T_2-weighted axial structural images were obtained over 15 adjacent 1-mm–thick slices using a fast spin echo sequence (acquisition time (TA) = 298 s, repetition time (TR) = 3.1 s, echo time (TE) = 67.5 ms, matrix (MTX) = 256 × 256, averages = 3, field of view (FOV) = 6 cm, rare factor = 8) under isoflurane anesthetic to give images with voxel size of 0.23 × 0.23 × 1 mm. Images were collected using Paravision 3.0 (Bruker Biospec).

Image analysis

Regions of interest (ROIs) were manually drawn around selected anatomic structures on each of the axial MR images (Fig. 1A), and the volume was calculated using Analyze (MAYO Foundation, Rochester, MN, U.S.A.). These structures included whole cerebrum, hippocampus, amygdala/piriform/entorhinal cortex, thalamus/hypothalamus, lateral ventricles, and cortex (including motor, somatosensory, auditory, visual, and parietal cortices) bilaterally. The FDG-PET image analysis was conducted as described previously (Liu et al., 2010). Each normalized FDG-PET volume was reformatted to have the same voxel size as the MRI volumes (i.e., 0.23 × 0.23 × 1 mm) with Analyze using a linear interpolation. The reformatted FDG-PET images were then manually coregistered to their corresponding MR image using the coregistration feature in Analyze (Fig. 1).

Manual coregistration involved aligning images to a visual "best-fit" based on six landmarks (harderian glands, olfactory bulbs, cerebral cortex, and cerebellum) in both the MRI and PET scans by a single operator who was blinded to treatment or imaging time point. This method was employed based on pilot data demonstrating that this method provided minimal error in registration when compared to automated

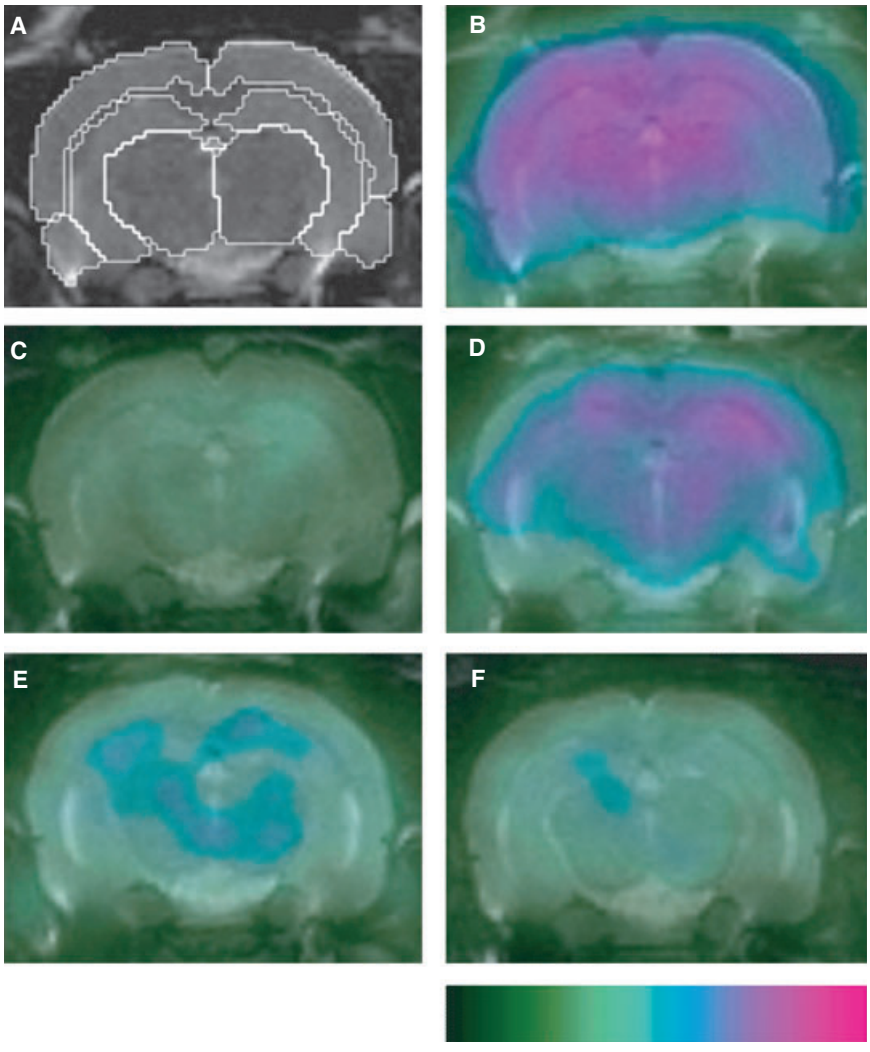

Figure 1.
Serial FDG-PET images of a KA-treated rat demonstrating the time course of cerebral hypometabolism following status epilepticus. (**A**) Coregistered MRI and FDG-PET demonstrating typical regions of interest. (**B**) Baseline FDG uptake. (**C**) Twenty-four hours after status epilepticus a significant decrease in glucose uptake is observed across the entire cerebrum. (**D**) One week after status epilepticus uptake is still decreased compared to baseline. (**E**) Three weeks after status epilepticus, uptake is further decreased when compared to 1 week after status epilepticus. (**F**) Five weeks after status epilepticus, FDG uptake is further decreased compared to weeks 1 and 3. Color bar at bottom of image indicates increasing FDG uptake from left to right.

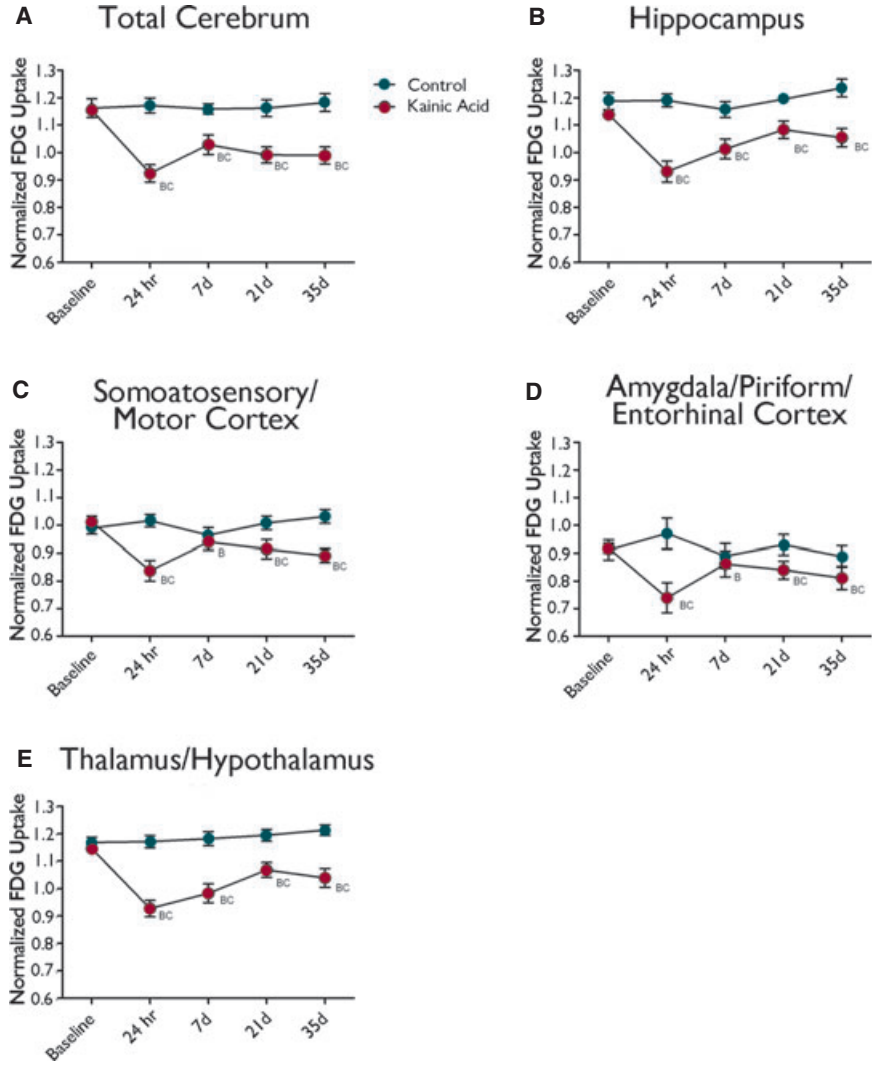

Figure 2.
Quantification of FDG uptake on PET in all regions examined in post-KA–induced status epilepticus animals. Total cerebral FDG uptake was reduced at 24 h following status epilepticus compared to control animals (**A**); this normalized at 1-week after status epilepticus in the somatosensory/motor cortices (**C**) and amygdala/piriform/entorhinal cortex (**D**) but was still significantly reduced compared to baseline. At all other time points examined, (7d, 21d, 35d post SE) all regions were significantly reduced when compared to both control and baseline values (**B**, **E**). $^{B}p < 0.05$ repeated measures ANOVA with planned comparisons, compared to baseline. $^{C}p < 0.05$ repeated measures ANOVA with planned comparisons, compared to control.
Epilepsia © ILAE

registration methods such as surface or voxel matching techniques (Jupp & O'Brien, 2007). ROIs drawn on MR images were then applied to each coregistered PET to obtain FDG uptake values for each structure.

Postmortem brain histologic processing

Following the final imaging session, animals were anesthetised (150 mg/kg ketamine 20 mg/kg xylazine, i.p.) and transcardially perfused with 100 mL 0.1 M phosphate-buffered saline (PBS), followed by 400 mL 4% paraformaldehyde in 0.1 M PBS. Brains were removed, postfixed in 4% paraformaldehyde, and cryoprotected in 20% sucrose in PBS before being frozen in Tissue Tek OCT (Sakura Fintek, Torrance, CA, U.S.A.) over liquid nitrogen and cryosectioned. Serial 20-μm coronal sections were collected onto Superfrost plus slides (Menzel-Glaser, Braunschweig, Germany), sampling the entire hippocampus between bregma −1.8 and −6.8 mm (Paxinos & Watson, 2005). Sections were allowed to air-dry overnight before being stored at −80°C until use.

Sections were used for stereologic estimation of hippocampal CA1 pyramidal cell number (status epilepticus treated, n = 8; control, n = 6) or for hippocampal, thalamic/hypothalamic, amygdala/entorhinal cortex immunoreactivity (IR) (based on ROIs from imaging studies) (status epilepticus treated, n = 5; control, n = 4) for markers of astrogliosis (glial fibrillary acidic protein [GFAP]), synaptogenesis (synaptophysin), glucose transporter 1 (Glut1), and energy metabolism (cytochrome oxidase C, COX-C). Because of technical issues in postmortem processing, resulting in sections of unsatisfactory quality, brains from three post-KA status epilepticus rats and one control rat were not included in the stereologic cell estimates, and brains from six post-KA rats and three controls were removed from the IR quantifications.

Quantification of hippocampal CA1 pyramidal cell numbers

Thionin staining was performed on every 10th section through the entire hippocampus to enable unbiased

stereologic assessment of CA1 pyramidal cell number for comparison with hippocampal FDG uptake. Briefly, slides were immersed in 0.1% thionin in acetate buffer solution (0.2 M acetic acid buffer) for 30 min before being dehydrated through an ascending ethanol series (water, 70%, 90%, 100% × 3) for 5 min per dilution. Slides were then cleared in histolene for 5 min and cover slipped with DPX (BDH Chemicals, Poole Dorset, United Kingdom).

A stereologic estimation of the total cell number in the left CA1 pyramidal cell layer using the optical fractionator method (West et al., 2001) was performed using Stereoinvestigator (MicroBrightField, Williston, VT, U.S.A.) on status epilepticus treated (n = 8) and control (n = 6) animals. The CA1 pyramidal cell layer was delineated using a 20× objective, and stereologic counts were performed with a 100× objective using a counting frame of dimension 25 × 25 × 6 μm and grid size of 250 × 250 μm by a reviewer blinded to the experimental group. This region was chosen based on previous studies suggesting it is most severely affected in the KA model and in TLE (Sharma et al., 2008; (de Lanerolle et al., 2003).

Immunohistochemistry

In addition, sections from control (n = 4) and status epilepticus treated (n = 5) animals were analyzed for alterations in left hippocampal, thalamic/hypothalamic, and amygdala/entorhinal cortex IR for markers of astrogliosis (GFAP), synaptogenesis (synaptophysin), Glut1, and energy metabolism (COX-C), using immunohistochemistry. Sections were processed for IR using an avidin–biotin peroxidase complex. Antibodies were used at the following dilutions: rabbit anti-GFAP (1:500; DAKO, Glostrup, Denmark), mouse anti-synaptophysin (1:100; Sigma-Aldrich, St. Louis, MO, U.S.A.), rabbit anti-Glut1 (1:100; AbCAM, Cambridge, United Kingdom), and mouse anti-COX-C (1:100; Invitrogen, Grand Island, NY, U.S.A.). The sections were incubated overnight and then incubated in the appropriate biotinylated secondary antibody (1:500; anti-mouse immunoglobulin G [IgG]; or anti-rabbit IgG; Vector Laboratories, Burlingame, CA, U.S.A.), followed by the avidin–biotin complex (1:500; Vector Laboratories), and reaction product visualized with 3,3′-diaminobenzidine (Sigma-Aldrich) in 0.01% hydrogen peroxide. For each antibody, all control and status epilepticus–treated animals were reacted simultaneously to minimize procedural variation. Control experiments were performed by omitting the primary antibodies; in these experiments, staining failed to occur, thereby confirming the specificity of biotin–avidin binding.

Images of immunostained sections were acquired by a reviewer blinded to treatment using a 20× objective under identical conditions (light levels and other microscopic settings) and saved as tagged image filed format files. Three images per section were taken over at least four sections sampling rostral, mid, and caudal regions of the structures of interest from bregma −3.3 to −6.8 mm to cover the regions analyzed in the imaging studies. An image was taken in the internal capsule for each section for normalization to account for variations in background staining intensity. Optical density (OD) measurements were taken in each image with manually drawn ROIs for the hippocampus, thalamus/hypothalamus, and the amygdala/entorhinal/piriform regions using MCID v4.0 (Interfocus Imaging, Cambridge, United Kingdom), corresponding anatomically with the ROIs for the MRI and PET image analyses. OD measurements in each region were normalized to the OD of the internal capsule to yield a relative optical density (ROD) for each region. Average RODs were calculated from the mean ROD of each region in each slice and then averaged across all slices. This average ROD was compared between epileptic and control animals.

Statistical analysis

All statistical tests were completed following advice from the Department of Mathematics and Statistics, The University of Melbourne. Significance was set at $p < 0.05$ for all tests. All data sets were subjected to a test of normality (Shapiro-Wilks) before performing appropriate statistical tests. Statistical differences between image signal intensity was examined between epileptic and control animals using repeated-measures analysis of variance (ANOVA) with planned comparisons. Differences between cell numbers and immunoreactive product between control and status epilepticus–treated animals were assessed using unpaired Student's *t*-tests. Any investigated correlations were performed using a Pearson's correlation. Where multiple correlations were observed, a stepwise backward multivariate regression analysis was performed to examine which factors independently predicted the variable being investigated.

Results

Kainic acid–induced SE results in early, persistent glucose hypometabolism on FDG-PET

There was a significant effect of status epilepticus on FDG uptake when compared to both baseline and control levels (Figs 1 and 2). Repeated-measures ANOVA showed a significant effect of time ($F_{4,340} = 14.969$; $p < 0.001$), treatment group ($F_{1,85} = 88.0$; $p < 0.001$), and brain region ($F_{4,85} = 52.349$; $p < 0.001$) on FDG uptake. Planned comparison analysis revealed a significant decrease in FDG uptake in total cerebrum and all subregions examined when compared to control and baseline, 24 h following SE and 21 and 35 days after status epilepticus. Seven days after status epilepticus, FDG uptake was still significantly reduced in total cerebrum and all regions examined compared to baseline and control uptake with the exception of the amygdala/piriform/entorhinal cortex region and somatosensory/motor cortices, which were no different from control levels but

were still significantly reduced compared to baseline uptake. A significant difference in uptake was also observed between the different regions of the brain between treatment groups. The amygdala/piriform/entorhinal cortex had significantly lower uptake in both control and post–status epilepticus animals than all other regions at all time points. The somatosensory/motor cortex also had significantly lower uptake than the hippocampus and thalamus/hypothalamus in both experimental groups.

Kainic acid–induced status epilepticus results in progressive atrophy of limbic structures and ventricular enlargement, but this does not correlate with the severity of FDG-PET hypometabolism

There were significant differences in the regional volumes between post–status epilepticus animals compared to controls (Fig. 3). Volumetric MR measures revealed a significant effect of time ($F_{4,320} = 12.57$; $p < 0.001$), and region ($F_{4,80} = 1151.509$; $p < 0.001$) and a significant interaction between time, region, and treatment ($F_{16,320} = 4.508$; $p < 0.001$). Planned comparisons revealed a significant decrease in the volume of the hippocampus and amygdala/piriform/entorhinal cortex in KA-treated animals ($p < 0.05$, repeated measures ANOVA with planned comparisons) compared to control animals. This decrease in the volume was significant from 7 days following status epilepticus (in the hippocampus) and progressed over the following 4 weeks during the epileptogenic period. In parallel with the decrease in limbic volume, there was a progressive significant increase in the lateral ventricular volume of the brain from 1 week following status epilepticus, which continued over the following 4 weeks. No significant change in volume was observed between KA and control animals in any other region investigated.

No significant correlations were observed at any imaging time point between the regional volumes and FDG-PET intensity for either the hippocampus or amygdala/piriform/entorhinal cortex ($p > 0.05$, Pearson's correlation, Table 1).

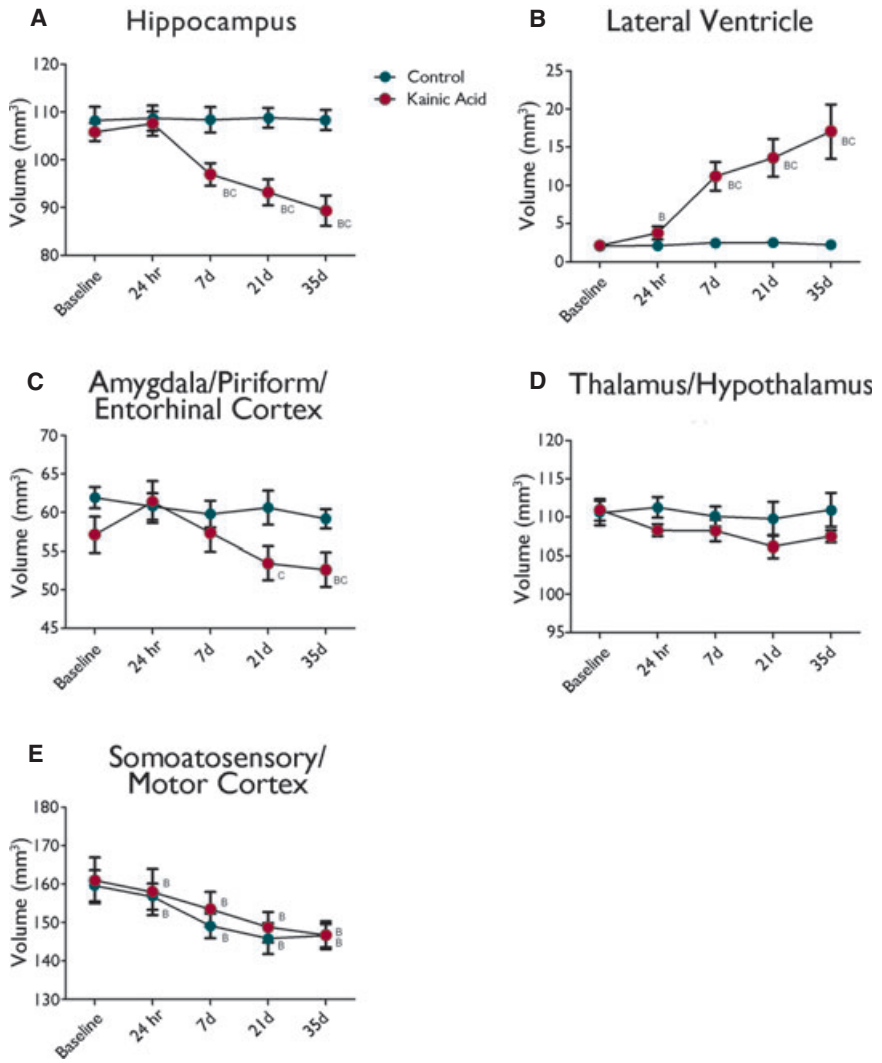

Figure 3.
Volumetric analysis of MR images in post-KA status epilepticus and control animals. Volume of the hippocampus (**A**), amygdala, and surrounding regions (**C**) is significantly reduced as early as 1 week following status epilepticus when compared to control animals and baseline measures. Corresponding increases in volume are observed in the lateral ventricle (**B**). A significant decrease compared to baseline volume is observed in the somatosensory and motor cortices for both post–status epilepticus and control animals (**E**), whereas the volume of the thalamic hypothalamic regions are unchanged (**D**). $^{B}p < 0.05$ repeated-measures ANOVA with planned comparisons, compared to baseline. $^{C}p < 0.05$ repeated-measures ANOVA with planned comparisons, compared to control. *Epilepsia* © ILAE

Table 1. R values for examined correlations between FDG-PET uptake and MRI volume in the hippocampus and amygdala and associated regions at each of the time points investigated

Region	24 h	1 week	3 weeks	5 weeks
Amygdala	−0.24	0.05	0.49	0.44
Hippocampus	0.02	0.5	0.7	0.7
Thalamus	0.53	0.51	0.38	−0.24
Cortex	−0.04	0.17	−0.07	0.17

The severity of hippocampal hypometabolism on FDG-PET is independently correlated with synaptophysin and glucose transporter 1 immunoreactivity but not hippocampal CA1 cell number

Unbiased stereologic estimations of the number of pyramidal cells in the CA1 region of the hippocampus revealed a significant reduction in animals with status epilepticus when compared to controls ($p < 0.05$, Student's *t*-test) (Fig. 4A). There was no significant correlation between pyramidal cell number in the CA1 region and the decrease in hippocampal glucose ($p > 0.05$, Pearson's correlations). No correlation was observed between pyramidal cell number in the CA1 region and hippocampal volume ($p > 0.05$, Pearson's correlation). The hippocampal IR for GFAP, synaptophysin, and Glut1 was found to be significantly increased in the post-KA animals (Fig. 4B–D), whereas COX-C IR was significantly decreased when compared to controls ($p < 0.05$, Student's *t*-tests) (Fig. 4E). There was a significant negative correlation between hippocampal FDG-PET intensity 5 weeks following status epilepticus and the ex vivo IR for GFAP, synaptophysin, and Glut1 at this time point (GFAP, $r = -0.67$; synaptophysin, $r = -0.93$, Glut1, $r = -0.77$, $p < 0.05$, Pearson's correlations) (Fig. 4). Multivariate regression analysis revealed that both Glut1 and synaptophysin IR were independently correlated with hippocampal FDG-PET intensity at 5 weeks post-KA ($B = -0.65, -0.89$ respectively, $p < 0.05$).

The severity of hypometabolism in extrahippocampal regions on FDG-PET does not correlate with IR for GFAP, synaptophysin, Glut1, and COX-C

The IR for GFAP, synaptophysin, Glut1, and COX-C was not different between post-KA status epilepticus and control animals in the two extrahippocampal regions examined, the thalamus/hypothalamus and the amygdala/entorhinal/pyriform regions ($p > 0.05$, Student's *t*-tests) (Fig. 5). In addition, there was no correlation between the IR for any of these markers and the severity of FDG-PET hypometabolism in either of these regions (all $p > 0.05$, Pearson's correlation).

Discussion

This study demonstrated that cerebral hypometabolism on FDG-PET is present early following status epilepticus

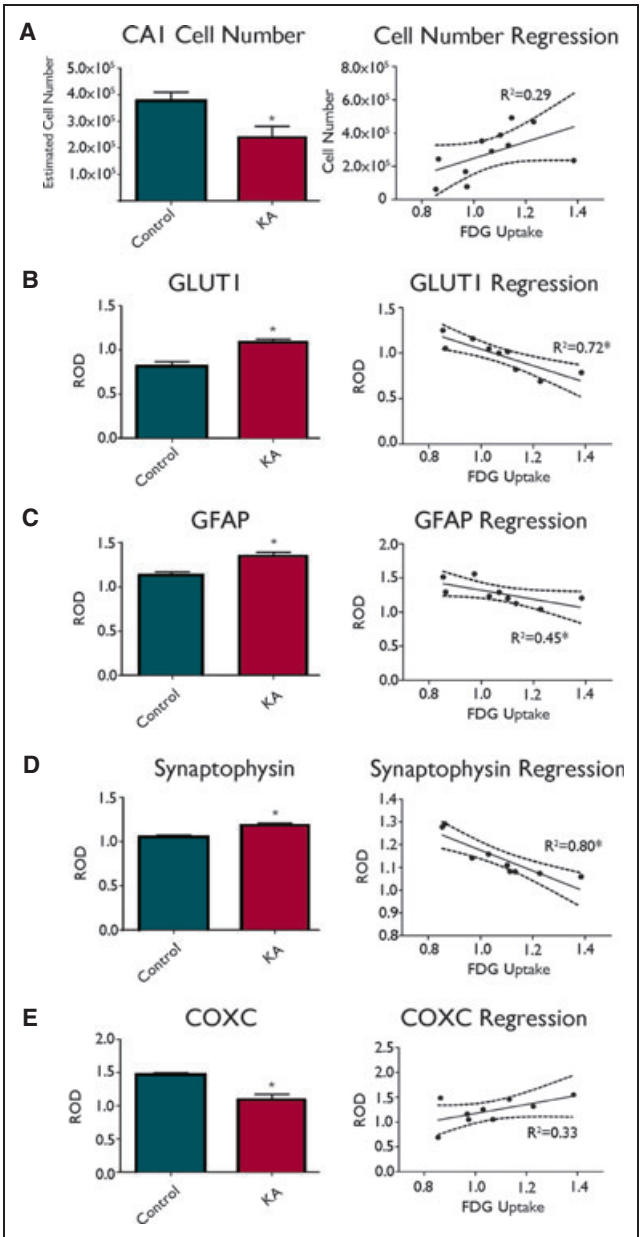

Figure 4.
Hippocampal histologic measures and their correlation to FDG-PET uptake at 35 days post-KA status epilepticus in the hippocampus. (**A**) The number of pyramidal cells in CA1 is reduced in post–status epilepticus rats; however, no correlation was observed between CA1 cell number and FDG uptake. GLUT1 (**B**), GFAP (**C**), and synaptophysin (**D**) hippocampal immunoreactivity were all increased in post-KA – rats and immunoreactivity negatively correlated with FDG-PET uptake for all of these markers. COX-C immunoreactivity was reduced in post–status epilepticus treated animals (**E**); however, this did not correlate with FDG-PET uptake. *$p < 0.05$, Student's *t*-test or Pearson's correlation.

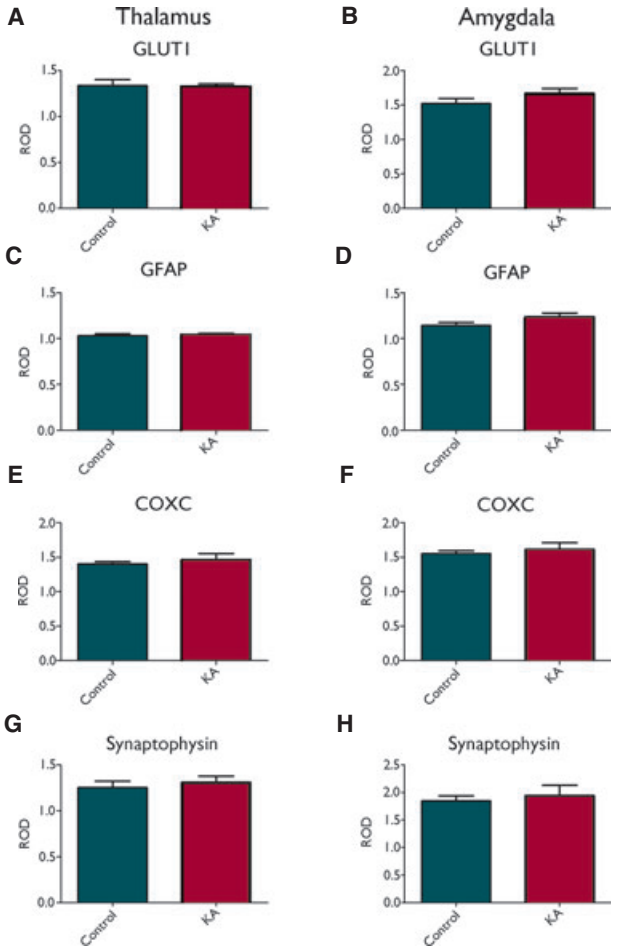

Figure 5.
Histologic measures in thalamic/hypothalamic and amygdala/entorhinal cortical regions of control and post-KA status epilepticus rats. No difference was observed in the immunoreactivity for GLUT1 (**A**, **B**), GFAP (**C**, **D**), synaptophysin (**E**, **F**), and COX-C (**G**, **H**) in the thalamus/hypothalamus (left hand side) or amygdala/entorhinal cortex (right hand side).

and persists during the epileptogenic period and following the onset of spontaneous recurrent seizures, suggesting that the hypometabolism is not entirely a consequence of chronic epilepsy and therefore may play an etiologic role in epileptogenesis. A spatiotemporal pattern of glucose uptake was also observed between the different regions investigated. The hippocampal and thalamic/hypothalamic regions showed a persistent reduction in glucose metabolism from as early as 24 h following status epilepticus, whereas FDG uptake in the amygdala/entorhinal cortex and motor/somatosensory cortices returned to control levels at 1 week following status epilepticus, only to decrease again at the later time points. This early appearance of hypometabolism confirms our previous report in this model (Jupp & O'Brien, 2007), and is consistent with those of other studies that have used serial FDG-PET studies or ex vivo 2-deoxyglucose autoradiography in the pilocarpine-induced status epilepticus model (Goffin et al., 2009; Guo et al., 2009). Guo et al. (2009) were able to provide evidence for the predictive nature of this early hypometabolism for the development of epilepsy, with a positive correlation observed between the degree of hypometabolism in the entorhinal cortex early following pilocarpine-induced SE and the later development of seizures. We were unable to examine such a correlation in our study because all of the animals developed spontaneous recurrent seizures within 5 weeks post-KA status epilepticus.

The temporal pattern of hypometabolism observed in the current study is suggestive of two distinct phases potentially reflecting different etiologies underlying the development of hypometabolism in this model of TLE; an initial reduction, which normalizes or tends to normalize by 1 week after status epilepticus, followed by a secondary reduction 3–5 weeks after status epilepticus with the emergence of spontaneous recurrent seizures. The initial decrease in glucose metabolism after status epilepticus possibly reflects the extended period of convulsive seizures experienced during status epilepticus and the massive energy demand associated with this. Indeed status epilepticus induces significant hypoxia (van Eijsden et al., 2004) and regional ischemia (Choy et al., 2010) within the brain, which has been demonstrated to result in glucose hypometabolism (Liu et al., 1997; Cheng et al., 2011). This disruption in neuronal metabolism, may contribute to structural and functional alterations responsible for the development of epilepsy as previously demonstrated (Guo et al., 2009). The secondary reduction in glucose metabolism, observed 3–5 weeks following status epilepticus, may reflect the effect of recurrent spontaneous seizures that increases progressively in frequency and severity post-KA status epilepticus (Williams et al., 2009) as well as alterations in the normal pattern of excitability within epileptic circuitry. In keeping with this, tissue hypoxia has been demonstrated to correlate with intensity of interictal spikes induced by bicuculline administration (Geneslaw et al., 2011), and there is evidence for anatomic concordance between interictal spiking and PET-detected hypometabolism (Person et al., 2010). Continued disturbance in neuronal metabolism may contribute to further structural and functional alterations as observed in the current study, which may in turn further disrupt the normal pattern of excitability within the brain. Indeed, there is increasing evidence to suggest that hypometabolism increases with longer epilepsy duration in TLE (Jokeit et al., 1999; Akman et al., 2010). This provides an attractive potential cellular mechanism for Gowers (1881) original hypothesis whereby ''seizures beget seizures,'' where the hypometabolism may both be a consequence of the seizures and contribute to their development. The differential spatiotemporal pattern of glucose uptake may indicate differences in the involvement of each of these regions in the

epileptogenic network, differences in the pathophysiology underlying the development of the hypometabolic state, or altered sensitivity to the effects of KA-induced status epilepticus.

Glucose hypometabolism and the contribution of neuronal loss

The underlying cause of temporal hypometabolism in patients with TLE has long been postulated to relate to neuronal cell loss associated with hippocampal sclerosis. A number of clinical studies have, however, failed to demonstrate significant correlation between hippocampal atrophy or neuronal density and glucose metabolism in patients with TLE (O'Brien et al., 1997; Theodore et al., 2001). Furthermore, patients without atrophy on MRI or significant surgically identified histologic cell loss often display marked temporal lobe hypometabolism (Carne et al., 2004). In the present study, significant progressive limbic volume loss was observed in the hippocampus and amygdala of animals following KA-induced status epilepticus on MRI, as has been reported in previous studies (Nakagawa et al., 2000; Wolf et al., 2002; Niessen et al., 2005; Nairismagi et al., 2006). These volumetric changes, however, did not correlate with the degree of hypometabolism on FDG-PET in any region or at any time point following status epilepticus. Furthermore, the onset of hypometabolism preceded the onset of significant volume loss and was observed in structures that failed to demonstrate any subsequent change in volume (i.e., the thalamus/hypothalamus). This finding agrees with results of our previous study in the fluid percussion model of head injury demonstrating no correlation between limbic atrophy and FDG-PET–detected hypometabolism (Liu et al., 2010). Hypometabolism was observed throughout the entire cerebrum rather than being limited to structures that sustain significant cell loss, although the limbic regions of amygdala/piriform/entorhinal cortex and hippocampus were more severely affected compared to nonlimbic regions.

Consistent with the lack of a relationship with the MRI volume measurements, no correlation was observed between the degree of hypometabolism in the hippocampus and the extent of pyramidal cell loss in the CA1 region of the hippocampus, the region that undergoes the majority of cell loss in this model of TLE (Sharma et al., 2008). Other regions displaying hypometabolism have also been reported to demonstrate neuronal loss in this model of TLE, for example, thalamus and amygdala (Chen & Buckmaster, 2005; Sharma et al., 2008), although in these studies, only specific nuclei within these regions were affected, and cell loss was relatively mild when compared to that observed in the hippocampus. In the present study we did not quantify neuronal cell numbers in these regions, and so cannot definitively state that no correlation exists between the cell loss and the hypometabolism. However, given the lack of a correlation between marked cell loss and the hypometabolism in the hippocampus, it seems unlikely that this was a major determinant underlying the hypometabolism seen in these other regions.

No correlation was observed between hippocampal CA1 neuronal loss and MRI hippocampal volumes, a finding that conflicts potentially with previous human studies (Lee et al., 1995; Briellmann et al., 2002). However, these previous studies utilized measurements of cell density rather than estimating total neuronal numbers in CA1 using unbiased stereologic techniques, as was done in the present study. In addition, although cell loss was quantified in the CA1 subregion, the MRI volumes encompassed the entire hippocampus. Significant neuronal loss has been reported in other hippocampal subregions of epileptic rats post-KA status epilepticus, in particular CA3 and the dentate hilus (Marksteiner et al., 1992; Brandt et al., 2003), and the relative cell loss in these subregions often differs considerably between animals, which could have confounded the correlation with the total hippocampal volumes. In a previous study using stereologic estimates, we found that neuronal loss in the CA3c region 24 h post-KA status epilepticus was of a magnitude similar to that seen in epileptic animals 6 weeks after status epilepticus (Vivash et al., 2011). This contrasts with the lack of change in hippocampal volumes seen in the present study at 24-h post-KA status epilepticus, and the progressive loss of volume seen at the later time points.

Cellular correlates of hypometabolism: cause or effect?

A number of histologic alterations commonly seen in the post-KA-induced status epilepticus model of TLE were also assessed for their relationship to glucose hypometabolism. An increase in the IR of GFAP, synaptophysin, and Glut1 was observed in the hippocampus of post-KA status epilepticus animals 5 weeks following status epilepticus, in accordance with previous reports in this and other models of TLE (Represa et al., 1995; Gronlund et al., 1996; Li et al., 2002). Independent correlations were observed between hypometabolism at 5 weeks after status epilepticus and synaptophysin and Glut1 IR. The correlations observed within the hippocampus may provide insight into a possible underlying cause/effect of hypometabolism in this structure, and they suggest mechanisms by which hypometabolism may contribute pathologically to the development of epilepsy. It is not possible to definitively confirm the cause-or-effect nature of these alterations, however, as only one time point after the development of the epilepsy was examined histologically.

Under normal circumstances, the major portion of glucose consumption in the brain is used for the maintenance of neuronal resting membrane potential (Mata et al., 1980; Huang et al., 2007). Disruption of glucose metabolism has been demonstrated to affect excitability within the brain (Wang et al., 2006; Stafstrom et al., 2009). Furthermore, it has been suggested that hypometabolism may reflect a decrease in postsynaptic inhibition (Pumain et al., 2008). Given this, it is likely that the disruption in glucose metabolism

observed after status epilepticus has significant effects on levels of excitability within the brain, which may in turn be responsible for the development and propagation of seizures via the hippocampus. Therefore, given the fact that hypometabolism was observed in this study early in the epileptogenic processes and the significant correlations between the magnitude of the hypometabolism and the changes in synaptogenesis and Glut1 IR, we postulate that the hypometabolism may be etiologically involved in the development of these cellular changes. For example the increase in Glut1, the main transporter of glucose across the blood–brain barrier, may occur in an attempt to increase the amount of glucose available to the brain to restore the balance required for normal resting membrane potential. Furthermore, there is evidence linking neuronal metabolic states to plasticity and synaptogenesis. Studies of hypoglycemic organotypic slices have demonstrated presynaptic remodeling typifying synaptogenesis (Nikonenko et al., 2003) and studies have shown that long-term potentiation can be regulated directly by neuronal energy metabolism (Potter et al., 2010). Therefore, hypometabolism may alter the underlying excitability of the hippocampus and contribute to the development of new synapses (and hence increased synaptophysin IR). This aberrant synaptogenesis may in turn further alter patterns of excitability.

No correlations between the IR for the studied markers and PET hypometabolism were observed in the two extrahippocampal regions examined. In addition, there were no differences in the IR for any of the markers between control and post–status epilepticus animals in these regions. This finding contrasts with that of previous studies in the post-KA–induced status epilepticus model, where astrogliosis has been observed (Gramsbergen & van den Berg, 1994; Sharma et al., 2008) within specific nuclei of the amygdala and thalamus. However, such subregion specific changes are likely to be lost in the large ROIs used in this study, which encompassed multiple nuclei, potentially diluting any specific effects. It should be noted that the lack of correlation in these regions may represent differences in the underlying cause/effect of hypometabolism, potentially reflecting the differential contribution of these regions to epileptogenesis. Clearly further investigation is required to determine whether the correlations observed within the hippocampus in the current study are specific to hypometabolism or represent unrelated epiphenomena.

Potential confounding effects of structural atrophy on the quantification of FDG-PET scans

The PET images acquired in this study were of lower resolution than those of the MR images. This can result in ''partial voluming effects'' in the PET ROIs with the image intensity in voxels covering gray matter regions reduced by inclusion of surrounding regions with low FDG uptake (e.g., ventricles). It is possible that this could have a confounding effect on the analysis if more of the ventricle was included in the PET ROIs of the post-KA status epilepticus animals (because of structural atrophy in this group). However, a number of factors argue against this being a major factor in the hypometabolism measured in the FDG-PET scans in the post-KA status epilepticus rats. First, the PET hypometabolism was most prominent in the scan acquired 24 h after the KA-induced status epilepticus, when neither the structural atrophy nor the increase in ventricular size was present on the MRI scans. Second, the structural brain atrophy in the hippocampus and amygdala/piriform/entorhinal regions, and increase in ventricular size, progressively increased over the three subsequent serial MRI scans, whereas this is not seen on the relevant PET quantifications for these regions. Third, relative hypometabolism was identified on the PET analysis in regions in which there was no significant atrophy seen on the MRI in the post-KA status epilepticus animals (i.e., the cortex and thalamus/hypothalamus). Finally, there was no significant correlation at any time point between the regional volumes and FDG-PET intensity for either the hippocampus or amygdala/piriform/entorhinal cortex ($p > 0.05$, Pearson's correlation, Table 1).

Conclusion

Serial FDG-PET and MRI during epileptogenesis post-KA status epilepticus demonstrated that cerebral glucose hypometabolism is present early following KA-induced status epilepticus, tends to normalize 1-week after status epilepticus, and then worsens again following the onset of spontaneous recurrent seizures. The severity of hypometabolism on FDG-PET does not correlate with the limbic atrophy or ventricular dilation that progressively develops over weeks following the status epilepticus in any of the regions investigated. A strong relationship was demonstrated, however, within the hippocampus between the degree of hypometabolism and the expression of the glucose transporter, GLUT-1, and a marker of synaptogenesis, synaptophysin. Taken together, these novel findings implicate that hypometabolism following an epileptogenic insult may occur as a result of, or result in, pathologic alterations, which may contribute to the processes of epileptogenesis.

Acknowledgments

The authors wish to thank Milosh Vosmanski, from Austin Health, Heidelberg, Victoria, Australia for the electrodes used in this study and Marnie Collins from the Department of Mathematics and Statistics, The University of Melbourne, for advice regarding the statistical analysis. The study was supported by the Australian Government funded CRC for Biomedical Development and a NHMRC Project Grant to TJ O'Brien and S Rees (#400088).

Disclosures

None of the authors has any conflict of interest to disclose.

We confirm that we have read the Journal's position on issues involved in ethical publication and affirm that this report is consistent with those guidelines.

References

Akman CI, Ichise M, Olsavsky A, Tikofsky RS, Van Heertum RL, Gilliam F. (2010) Epilepsy duration impacts on brain glucose metabolism in temporal lobe epilepsy: results of voxel-based mapping. *Epilepsy Behav* 17:373–380.

Brandt C, Potschka H, Loscher W, Ebert U. (2003) *N*-methyl-D-aspartate receptor blockade after status epilepticus protects against limbic brain damage but not against epilepsy in the kainate model of temporal lobe epilepsy. *Neuroscience* 118:727–740.

Briellmann RS, Kalnins RM, Berkovic SF, Jackson GD. (2002) Hippocampal pathology in refractory temporal lobe epilepsy: T2-weighted signal change reflects dentate gliosis. *Neurology* 58:265–271.

Carne RP, O'Brien TJ, Kilpatrick CJ, MacGregor LR, Hicks RJ, Murphy MA, Bowden SC, Kaye AH, Cook MJ. (2004) MRI-negative PET-positive temporal lobe epilepsy: a distinct surgically remediable syndrome. *Brain* 127:2276–2285.

Chen S, Buckmaster PS. (2005) Stereological analysis of forebrain regions in kainate-treated epileptic rats. *Brain Res* 1057:141–152.

Cheng F, Xie S, Guo M, Fang H, Li X, Yin J, Lu G, Li Y, Ji X, Yu S. (2011) Altered glucose metabolism and preserved energy charge and neuronal structures in the brain of mouse intermittently exposed to hypoxia. *J Chem Neuroanat* 42:65–71.

Choy M, Wells JA, Thomas DL, Gadian DG, Scott RC, Lythgoe MF. (2010) Cerebral blood flow changes during pilocarpine-induced status epilepticus activity in the rat hippocampus. *Exp Neurol* 225:196–201.

Dedeurwaerdere S, Jupp B, O'Brien TJ. (2007) Positron emission tomography in basic epilepsy research: a view of the epileptic brain. *Epilepsia* 48:56–64.

de Lanerolle NC, Kim JH, Williamson A, Spencer SS, Zaveri HP, Eid T, Spencer DD. (2003) A retrospective analysis of hippocampal pathology in human temporal lobe epilepsy: evidence for distinctive patient subcategories. *Epilepsia* 44:677–687.

Fink GR, Pawlik G, Stefan H, Pietrzyk U, Wienhard K, Heiss WD. (1996) Temporal lobe epilepsy: evidence for interictal uncoupling of blood flow and glucose metabolism in temporomesial structures. *J Neurol Sci* 137:28–34.

Foldvary N, Lee N, Hanson MW, Coleman RE, Hulette CM, Friedman AH, Bej MD, Radtke RA. (1999) Correlation of hippocampal neuronal density and FDG-PET in mesial temporal lobe epilepsy. *Epilepsia* 40:26–29.

Geneslaw AS, Zhao M, Ma H, Schwartz TH. (2011) Tissue hypoxia correlates with intensity of interictal spikes. *J Cereb Blood Flow Metab* 31:1394–1402.

Goffin K, Van Paesschen W, Dupont P, Van Laere K. (2009) Longitudinal microPET imaging of brain glucose metabolism in rat lithium-pilocarpine model of epilepsy. *Exp Neurol* 217:205–209.

Gonzalez-Lima F. (1992) Brain imaging of auditory learning funtions in rats: study with fluorodeoxyglucose autoradiography and cytochrome oxidase histochemistry. In Gonzalez-Lima F, Finkenstadt T, Scheich H (Eds) *Advances in metabolic mapping techniques for brain imaging of behavioral and learning functions*. Kluwer, Boston, pp. 39–109.

Gowers WG. (1881) *Epilepsy and other chronic convulsive disorders: their causes, symptoms and treatment*. Churchill, London.

Gramsbergen JB, van den Berg KJ. (1994) Regional and temporal profiles of calcium accumulation and glial fibrillary acidic protein levels in rat brain after systemic injection of kainic acid. *Brain Res* 667:216–228.

Gronlund KM, Gerhart DZ, Leino RL, McCall AL, Drewes LR. (1996) Chronic seizures increase glucose transporter abundance in rat brain. *J Neuropathol Exp Neurol* 55:832–840.

Guo Y, Gao F, Wang S, Ding Y, Zhang H, Wang J, Ding MP. (2009) In vivo mapping of temporospatial changes in glucose utilization in rat brain during epileptogenesis: an 18F-fluorodeoxyglucose-small animal positron emission tomography study. *Neuroscience* 162:972–979.

Hellier JL, Dudek FE. (2005) Chemoconvulsant model of chronic spontaneous seizures. *Curr Protoc Neurosci* Chapter 9:Unit 9 19.

Hellier JL, Patrylo PR, Buckmaster PS, Dudek FE. (1998) Recurrent spontaneous motor seizures after repeated low-dose systemic treatment with kainate: assessment of a rat model of temporal lobe epilepsy. *Epilepsy Res* 31:73–84.

Henry TR, Mazziotta JC, Engel J Jr, Christenson PD, Zhang JX, Phelps ME, Kuhl DE. (1990) Quantifying interictal metabolic activity in human temporal lobe epilepsy. *J Cereb Blood Flow Metab* 10: 748–757.

Huang CW, Huang CC, Cheng JT, Tsai JJ, Wu SN. (2007) Glucose and hippocampal neuronal excitability: role of ATP-sensitive potassium channels. *J Neurosci Res* 85:1468–1477.

Jokeit H, Ebner A, Arnold S, Schuller M, Antke C, Huang Y, Steinmetz H, Seitz RJ, Witte OW. (1999) Bilateral reductions of hippocampal volume, glucose metabolism, and wada hemispheric memory performance are related to the duration of mesial temporal lobe epilepsy. *J Neurol* 246:926–933.

Jupp B, O'Brien TJ. (2007) Application of coregistration for imaging of animal models of epilepsy. *Epilepsia* 48(Suppl. 4):82–89.

Jupp B, Williams JP, Tesiram YA, Vosmansky M, O'Brien TJ. (2006a) Hippocampal T2 signal change during amygdala kindling epileptogenesis. *Epilepsia* 47:41–46.

Jupp B, Williams JP, Tesiram YA, Vosmansky M, O'Brien TJ. (2006b) MRI compatible electrodes for the induction of amygdala kindling in rats. *J Neurosci Methods* 155:72–76.

Kornblum HI, Araujo DM, Annala AJ, Tatsukawa KJ, Phelps ME, Cherry SR. (2000) In vivo imaging of neuronal activation and plasticity in the rat brain by high resolution positron emission tomography (microPET). *Nat Biotechnol* 18:655–660.

Lee N, Tien RD, Lewis DV, Friedman AH, Felsberg GJ, Crain B, Hulette C, Osumi AK, Smith JS, VanLandingham KE, Radtke RA. (1995) Fast spin-echo, magnetic resonance imaging-measured hippocampal volume: correlation with neuronal density in anterior temporal lobectomy patients. *Epilepsia* 36:899–904.

Li S, Reinprecht I, Fahnestock M, Racine RJ. (2002) Activity-dependent changes in synaptophysin immunoreactivity in hippocampus, piriform cortex, and entorhinal cortex of the rat. *Neuroscience* 115:1221–1229.

Liu Y, Mituska S, Hashizume K, Hosaka T, Nukui H. (1997) The sequential change of local cerebral blood flow and local cerebral glucose metabolism after focal cerebral ischaemia and reperfusion in rat and the effect of MK-801 on local cerebral glucose metabolism. *Acta Neurochir (Wien)* 139:770–779.

Liu YR, Cardamone L, Hogan R, Gregoire M-C, Williams JP, Hicks RJ, Binns DS, Koe A, Jones NC, Myers DE, O'Brien TJ, Bouilleret V. (2010) Progressive metabolic and structural cerebral perturbations following traumatic brain injury: an in vivo imaging study in the rat. *J Nucl Med* 51:1788–1795.

Marksteiner J, Wahler R, Bellmann R, Ortler M, Krause JE, Sperk G. (1992) Limbic seizures cause pronounced changes in the expression of neurokinin B in the hippocampus of the rat. *Neuroscience* 49:383–395.

Mata M, Fink DJ, Gainer H, Smith CB, Davidsen L, Savaki H, Schwartz WJ, Sokoloff L. (1980) Activity-dependent energy metabolism in rat posterior pituitary primarily reflects sodium pump activity. *J Neurochem* 34:213–215.

Matheja P, Kuwert T, Ludemann P, Weckesser M, Kellinghaus C, Schuierer G, Diehl B, Ringelstein EB, Schober O. (2001) Temporal hypometabolism at the onset of cryptogenic temporal lobe epilepsy. *Eur J Nucl Med* 28:625–632.

Mirrione MM, Schiffer WK, Siddiq M, Dewey SL, Tsirka SE. (2006) PET imaging of glucose metabolism in a mouse model of temporal lobe epilepsy. *Synapse* 59:119–121.

Nairismagi J, Pitkanen A, Kettunen MI, Kauppinen RA, Kubova H. (2006) Status epilepticus in 12-day-old rats leads to temporal lobe neurodegeneration and volume reduction: a histologic and MRI study. *Epilepsia* 47:479–488.

Nakagawa E, Aimi Y, Yasuhara O, Tooyama I, Shimada M, McGeer PL, Kimura H. (2000) Enhancement of progenitor cell division in the dentate gyrus triggered by initial limbic seizures in rat models of epilepsy. *Epilepsia* 41:10–18.

Niessen HG, Angenstein F, Vielhaber S, Frisch C, Kudin A, Elger CE, Heinze HJ, Scheich H, Kunz WS. (2005) Volumetric magnetic resonance imaging of functionally relevant structural alterations in chronic epilepsy after pilocarpine-induced status epilepticus in rats. *Epilepsia* 46:1021–1026.

Nikonenko I, Jourdain P, Muller D. (2003) Presynaptic remodeling contributes to activity-dependent synaptogenesis. *J Neurosci* 23:8498–8505.

O'Brien TJ, Newton MR, Cook MJ, Berlangieri SU, Kilpatrick C, Morris K, Berkovic SF. (1997) Hippocampal atrophy is not a major determinant of regional hypometabolism in temporal lobe epilepsy. *Epilepsia* 38:74–80.

O'Brien TJ, Hicks RJ, Ware R, Binns DS, Murphy M, Cook MJ. (2001) The utility of a 3-dimensional, large-field-of-view, sodium iodide crystal–based PET scanner in the presurgical evaluation of partial epilepsy. *J Nucl Med* 42:1158–1165.

O'Brien TJ, Miles K, Ware R, Cook MJ, Binns DS, Hicks RJ. (2008) The cost-effective use of 18F-FDG PET in the presurgical evaluation of medically refractory focal epilepsy. *J Nucl Med* 49:931–937.

Paxinos G, Watson C. (2005) *The rat brain in stereotaxic coordinates*. Elsevier Academic Press, Sydney.

Person C, Koessler L, Louis-Dorr V, Wolf D, Maillard L, Marie PY. (2010) Analysis of the relationship between interictal electrical source imaging and PET hypometabolism. *Conf Proc IEEE Eng Med Biol Soc* 2010:3723–3726.

Potter WB, O'Riordan KJ, Barnett D, Osting SM, Wagoner M, Burger C, Roopra A. (2010) Metabolic regulation of neuronal plasticity by the energy sensor AMPK. *PLoS ONE* 5:e8996.

Pumain R, Ahmed MS, Kurcewicz I, Trottier S, Louvel J, Turak B, Devaux B, Laschet J. (2008) Lability of GABAA receptor function in human partial epilepsy: possible relationship to hypometabolism. *Epilepsia* 49:7–90.

Represa A, Niquet J, Pollard H, Ben-Ari Y. (1995) Cell death, gliosis, and synaptic remodeling in the hippocampus of epileptic rats. *J Neurobiol* 26:413–425.

Sharma AK, Jordan WH, Reams RY, Hall DG, Snyder PW. (2008) Temporal profile of clinical signs and histopathologic changes in an F-344 rat model of kainic acid-induced mesial temporal lobe epilepsy. *Toxicol Pathol* 36:932–942.

Stafstrom CE, Ockuly JC, Murphree L, Valley MT, Roopra A, Sutula TP. (2009) Anticonvulsant and antiepileptic actions of 2-deoxy-D-glucose in epilepsy models. *Ann Neurol* 65:435–447.

Theodore WH, Gaillard WD, De Carli C, Bhatia S, Hatta J. (2001) Hippocampal volume and glucose metabolism in temporal lobe epileptic foci. *Epilepsia* 42:130–132.

van Eijsden P, Notenboom RG, Wu O, de Graan PN, van Nieuwenhuizen O, Nicolay K, Braun KP. (2004) In vivo 1H magnetic resonance spectroscopy, T2-weighted and diffusion-weighted MRI during lithium-pilocarpine-induced status epilepticus in the rat. *Brain Res* 1030:11–18.

Vivash L, Tostevin A, Liu DS, Dalic L, Dedeurwaerdere S, Hicks RJ, Williams DA, Myers DE, O'Brien TJ. (2011) Changes in hippocampal GABAA/cBZR density during limbic epileptogenesis: relationship to cell loss and mossy fibre sprouting. *Neurobiol Dis* 41:227–236.

Wang Y, Zaveri H, Ghosh A, Beckstrom J, de Lanerolle N, Eid T. (2006) Inhibition of hippocampal glutamine synethetase causes spontaneously recurrent seizures in rats. *American Epilepsy Society Meeting*, San Diego, CA, U.S.A., 4.112.

West M., Slomianka L., Gundersen HJG. (1991) Unbiased stereological estimation of the total number of neurons in the subdivisions of the rat hippocampus using the optical fractionator. *Anatomical Record* 231:482–497.

Williams PA, White AM, Clark S, Ferraro DJ, Swiercz W, Staley KJ, Dudek FE. (2009) Development of spontaneous recurrent seizures after kainate-induced status epilepticus. *J Neurosci* 29:2103–2112.

Wolf OT, Dyakin V, Patel A, Vadasz C, de Leon MJ, McEwen BS, Bulloch K. (2002) Volumetric structural magnetic resonance imaging (MRI) of the rat hippocampus following kainic acid (KA) treatment. *Brain Res* 934:87–96.